Published in final edited form as:
Int Forum Allergy Rhinol. 2014 June ; 4(6): 435–446. doi:10.1002/alr.21319.

What is normal nasal airflow? A computational study of 22 healthy adults

Kai Zhao, Ph.D and **Jianbo Jiang, Ph.D.**
Monell Chemical Senses Center, Philadelphia, USA, and (KZ) Department of Otolaryngology, Thomas Jefferson University, Philadelphia, PA, USA

Abstract

Objective—Nasal airflow is essential for functioning of the human nose. Given individual variation in nasal anatomy, there is yet no consensus what constitutes normal nasal airflow patterns. We attempt to obtain such information that is essential to differentiate disease-related variations.

Methods—Computational fluid dynamics (CFD) simulated nasal airflow in 22 healthy subjects during resting breathing. Streamline patterns, airflow distributions, velocity profiles, pressure, wall stress, turbulence, and vortical flow characteristics under quasi-steady state were analyzed. Patency ratings, acoustically measured minimum cross-sectional area (MCA), and rhinomanometric nasal resistance (NR) were examined for potential correlations with morphological and airflow-related variables.

Results—Common features across subjects included: >50% total pressure-drop reached near the inferior turbinate head; wall shear stress, NR, turbulence energy, and vorticity were lower in the turbinate than in the nasal valve region. However, location of the major flow path and coronal velocity distributions varied greatly across individuals. Surprisingly, on average, more flow passed through the middle than the inferior meatus and correlated with better patency ratings ($r=-0.65$, $p<0.01$). This middle flow percentage combined with peak post-vestibule nasal heat loss and MCA accounted for >70% of the variance in subjective patency ratings and predicted patency categories with 86% success. Nasal index correlated with forming of the anterior dorsal vortex. Expected for resting breathing, the functional impact for local and total turbulence, vorticity, and helicity was limited. As validation, rhinomanometric NR significantly correlated with CFD simulations ($r=0.53$, $p<0.01$).

Conclusion—Significant variations of nasal airflow found among healthy subjects; Key features may have clinically relevant applications.

INTRODUCTION

Airflow in the human nose is critical for its physiological functions, including filtering and conditioning inhaled air, respiration feedback, and the sense of smell and irritation[1]. Nasal

Corresponding author: Kai Zhao Monell Chemical Senses Center Philadelphia, PA 19104 267-519-4935 (phone and fax) kzhao@monell.org, zhaok@alumni.upenn.edu.

Conflicts of interest: “none.”

airflow patterns are determined mainly by the anatomical structures of the nose and breathing conditions. Not surprisingly, human nasal anatomy differs significantly from person to person. In addition, various types of nasal diseases, such as inflammation, allergy, sinusitis, and polyps, can also affect nasal airflow. Thus, understanding the normal variations in nasal airflow, patterns, and related transport phenomena is essential for differentiating disease-related alterations of nasal airflow.

Considerable work, both experimental and numerical, has been devoted to the investigation of human nasal airflow, mainly focusing on small numbers of subjects. However, ongoing controversies remain regarding the major flow path, flow regime (laminar, transitional, or turbulent), and existence and locations of vortices (flow separation). The major nasal airflow during quiet inspiration was found in the space between the middle turbinate and the nasal septum in some experiments[2;3] but in the inferior meatus[4-6] or middle meatus[7] in other experiments. In a computational fluid dynamics (CFD) study, Zhao et al.[8] found a different major flow path in the left and right nasal cavity of the same healthy person. Laminar flow was commonly assumed in most CFD studies of human nasal airflow during quiet breathing[5;8;9], with experimental support[6;10;11]. In contrast, transitional or even turbulent flows were reported by some researchers[3;12;13]. As a result of separate flows, a vortex was found in the vestibule and nasopharynx area in the CFD study of Subramaniam et al.[9], and in the olfactory area in the experiments of Swift and Proctor[2] and Schreck et al.[13], but not in the experimental studies of Kelly et al.[6] and Chung et al.[7] or the CFD study of Keyhani et al.[5].

These discrepancies are most likely due to the different nasal models adopted in these studies. Churchill et al.[14] experimentally investigated the major flow path and flow regime by flowing water and dye through nasal replicas of 10 Caucasian (‘‘leptorrhine’’) cadavers. They found that both flow regimes and major flow pathways were highly variable within their sample. No laminar flow was observed even at the lowest flow rate of 0.1 L/min, but the major flow path was below the middle meatus. Segal et al.[15] studied the airflow pattern during restful breathing in four nasal CFD models from healthy subjects and found significant differences in swirling flow and regional flow distributions among them. The major flow path was, however,found in either the middle (3 of 4) or ventral (1 of 4) regions of the nasal airways. In a recent paper, Zhu et al.[16] compared the nasal airflow pattern during restful breathing in three healthy male subjects from Caucasian, Chinese, and Indian ethnic groups using CFD techniques. The main flow path was found in the middle meatuses of the Caucasian model, inferior common meatus of the Chinese model, and middle common meatus of the Indian model. However, whether these reported nasal airflow variations have any impact on nasal functions remains unclear and has not been touched upon by any previous studies.

The objective of this study was to extend a prior study[17] to quantify variations of nasal geometry and airflow patterns in a cohort of healthy subjects by using CFD techniques. Twenty-two anatomically accurate three-dimensional computational nasal models were developed from computed tomography (CT) scans. Inspiratory flows under restful breathing were simulated, and detailed velocity profiles, volumetric flow distributions, streamline patterns, pressure, turbulent energy, and wall shear stress were presented to allow qualitative

and quantitative comparisons among the individuals. As described previously[17], nasal patency ratings in room air using a visual analog scale (VAS), rhinomanometry and acoustic rhinometry measurements were available for these subjects. External nose shape was also measured by nasal index. One of the open criticisms in the field regarding nasal airflow modeling and computational studies is that whether or not these simulated internal and external nasal airflow features really affected nasal functions or have any impact on clinical outcomes. So next, we attempted to correlate the nasal airflow and morphological variables obtained in this study with subjective nasal patency ratings, an important clinical outcome variable. To collect preliminary data for future translational applications, we further attempted to predict nasal patency perception categories (normal vs. obstruction) based on the significant variables from the correlation analysis. Ultimately, these findings can potentially be translated to clinical populations to formulate hypothesis and to separate effects of normal anatomical variations from those of pathological origin on nasal airflow and to fully understand the impact of nasal sinus disease on nasal conductive functions.

METHODS

Subjects

This study is a continuation of a published study, where 22 healthy subjects underwent CT scans for CFD modeling[17]. The group consisted of 10 males and 12 females: 20 Caucasian, 1 African American, and 1 Asian American. Their ages ranged from 21 to 39 years, with a mean of 25.6, median of 24.5, and standard deviation of 4.84 years. The study was approved by the institutional review boards of both the University of Pennsylvania and Thomas Jefferson University. Written informed consent was obtained from all volunteers. All of the participants underwent medical history screening to exclude pre-existing nasal sinus disease, prior nasal sinus complaint, head trauma, and prior nasal surgery. Both acoustic rhinometry and rhinomanometry were performed immediately before the CT scan on all subjects to objectively confirm the absence of severe nasal obstruction. Two additional subjects failed to complete the study protocol and were not included in the final data set.

Rhinometry

The minimum (narrowest) cross-sectional area (MCA) in the anterior 5 cm of nasal airway was collected unilaterally using an acoustic rhinometry (SRE21000, RhinoMetrics A/S, Denmark) for each subject. The MCA from both sides were summed as the bilateral MCA. Unilateral nasal resistance[18] during normal breathing was measured by anterior rhinomanometry (SRE21000, RhinoMetrics A/S) at a reference pressure drop of 75 Pa. Bilateral nasal resistance is calculated based on unilateral resistance of the two sides: $1/R_{total} = 1/R_{left} + 1/R_{right}$. The rhinomanometry measurement for one subject was not correctly performed due to staff error; the sample size is thus reduced (n=21) in analyses that include nasal resistance.

Nasal index

Using CT-reconstructed facial features (see Figure 1), the nasal index was determined as the ratio of the external nasal width and height. The nasal index is often used in anthropological studies to classify human race based on the external shape and size of their nose:

"leptorrhine" (narrow-nosed), "mesorrhine" (medium-nosed), or "platyrrhine" (broad-nosed). These differences have been proposed to be an adaptation to climate, with broad noses (platyrrhine) evolving in warm, humid environments where there is little need for air conditioning and narrow noses (leptorrhine) evolving in colder climates where the air needs more warming[19]. There has been some interest in the rhinology field in predicting nasal physiology and its susceptibility to nasal sinus disease by easily obtainable external physical measurements[20;21]. Here, we examined the relationship between intranasal airflow feature and nasal index.

Nasal patency ratings

As previously described[22], bilateral nasal patency was rated by each subject using a visual analog scale (VAS; 0, completely clear – 10, completely congested) while sampling air from the exposure boxes that were ventilated with room air. The whole procedure was repeated to examine test-retest reliability, after which the two ratings were averaged. While the effect of air humidity, temperature, and nasal mucosal heat loss on unilateral patency ratings has already been published[22], here we examined potential relationships between bilateral nasal patency and the additional variables related to internal and external nasal airflow and morphology obtained in this study.

CT scan and CFD model

Following rhinometry measurements and patency ratings at the Monell Chemical Senses Center, participants were immediately escorted by staff to Thomas Jefferson University Hospital (Philadelphia, PA), via a 10- to 15-min subway ride, to undergo a spiral sinus CT. The CT enabled the construction of "real-time" CFD nasal airway models for each subject using methods described previously[8]. In brief, the scans were imported into the commercial software AMIRA (Visualization Sciences Group, USA) to extract nasal cavity geometry. After necessary segmentation, smoothing, and correction for artifacts, a three-dimensional surface geometry of the nasal airway was generated. All sinuses were included in the CFD model, as long as they were shown to be open to the main nasal airway based on the CT scan. Then the commercial grid generator ICEM CFD (Ansys, Inc., USA) was applied to generate the mesh. In order to resolve the boundary layer, a thin (~0.2 mm) region consisting of four layers compact hybrid tetrahedral/pentahedral elements was generated near the surface[8]. The thickness of each layers follow power growth law that the second layer is 1.2 times thicker than the first layer, etc. A typical initial nasal cavity mesh after boundary layers contained between 1 million and 3 million hybrid finite elements. Then the initial meshes were refined by gradient adaptation and boundary adaptation until grid independence of the solutions was achieved. The dimensionless distance for wall-bounded flow (y^+) were further examined to ensure that it was within the first wall cell. The final grids contained approximately 1.8 million to 3.5 million elements.

The solutions of the three-dimensional steady Navier-Stokes and continuity equations were obtained using the commercial software package FLUENT 13.1 (Ansys, Inc.). As described in the Introduction, whether human nasal airflow during restful breathing (flow rate <200 ml/s) is turbulent is still an open question. So the low-Reynolds-number k-ω turbulence model was used to simulate the flow field with a turbulence intensity of 2.5%[11] of the mean

velocity imposed at inlet location and compared with the laminar model to investigate possible turbulence effects. The low-Reynolds-number k-ω turbulent model has been shown to be valid, and reliable in the prediction of laminar, transitional, and turbulent flow behavior[23]. Along the nasal walls, the usual no-slip velocity condition was applied, and the wall is assumed to be rigid. At the nasopharynx, the "pressure outlet" condition was adopted. At the external naris, pressure inlet with pressure drop of 15 Pa was imposed as the driving force of airflow through the nose. The resulting inhalation rate was <200 ml/s, within the restful breathing range.

The numerical solutions of the continuity, momentum, and/or turbulence transport equations were determined using the finite-volumes method. A second-order upwind scheme was used for spatial discretization. The SIMPLEC algorithm was used to link pressure and velocity. The discretized equations were then solved sequentially using a segregated solver. Convergence was obtained when the scaled residuals of continuity, momentum, and/or turbulence quantities were $<10^{-5}$. Global quantities such as flow rate and pressure on the nasal walls were further monitored to check the convergence.

RESULTS

Nasal Morphology, Pressure Drop, and Nasal Resistance

We first compared nasal morphology among the 22 subjects. Table 1 lists the values of total surface area and total volumes for each subject, which were calculated from the external nostrils to the end of the septum, excluding the nasopharynx. Although volume and surface area vary significantly (~ 2 times) across individuals, they strongly correlate with each other (see Figure 2a). No correlation was found between nasal surface, volume, or surface-to-volume ratio and any other variables obtained in this study. We further examined nasal morphology changes from nostrils to pharynx. To account for different overall lengths of different noses, each nasal cavity was sectioned into 19 uniformly spaced coronal planes (see Figure 2b). The last three coronal sections that cut through the nasopharynx region were excluded from the analysis. Cross-sectional area was generally smallest in the nasal valve region and expanded in the turbinate and nasopharynx regions (Figure 2c,d). Sinuses contributed significantly more cross-sectional area and volume (2.05 times on average) than did the main nasal airway.

Cross-sectional averaged air pressure from both laminar and turbulent simulations decreased along the nasal airway (laminar simulation results shown in Figure 2e). On average, >50% of the pressure drop was reached at the nasal valve region. The distance between the nostril tip and the inferior head is in the range of 0.28-0.37*L*, where *L* is averaged length of the nasal cavity (Figure 2b). The pressure drop between the naris and inferior head accounted for ~50-73% of the total pressure drop. CFD-simulated internal nasal resistance (based on internal pressure loss) correspondingly was also highest in the nasal valve region and decreased as the nasal airway expanded (Figure 2f). The rhinomanometrically measured total nasal resistance showed significant variations among subjects (Table 2). However, the (0.065, SD 0.029 Pa/ml/s) are comparable to those of normal subjects reported in the literature: Warren et al.[24] (0.09-0.3 Pa/ml/s; flow rate, 500 ml/s), Moore and Kern[25] (0.15-0.3; pressure drop, 150 Pa), and Eccles[26](<0.3; 150 Pa). Wall shear stress also peaked

at the nasal valve region in patterns similar to those for nasal resistance. As a crude validation, rhinomanometry-measured nasal resistances significantly correlated with CFD-simulated ones ($r=0.53$, $p<0.01$, see Table 3).

Streamlines, Vortices, and Nasal Index

Streamlines were used to visualize the flow patterns inside the nasal cavity. For every nasal cavity, 1,000 neutral-buoyant particles were uniformly released on the nostril plane to track their streamlines, and further increasing the number of released particles did not provide further information. While various features of the airflow streamline patterns across the subjects were found, the most striking variation is the forming of the anterior dorsal vortex, right after the nasal valve, which was first reported by Swift and Proctor[2]. Figure 3 shows examples of (a) no vortex, (b) a small vortex, (c) a significant vortex, and (d) a significant vortex but in clockwise rotation. The forming of the vortex likely depends on the angle of the nasal valve and abrupt volume increase after the nasal valve. To examine this, we scored each nasal cavity for anterior dorsal vortex using Figure 3 as template: no vortex = 0 (a), small = 1 (b), large = 2 (c and d), and the scores for the two sides were summed for each subject. The distribution of the score in the sample group (0, n=8; 1-3, n=11; 4, n=3) indicates that the forming of such vortices is quite common in this healthy cohort. A significant correlation was found between vortex score and nasal index ($r=-0.46$, $p<0.05$), which indicates that a narrower and taller external nose is more likely to have flow separation and form the vortex. The exact functional relevance of these anterior dorsal vortices is unclear, as no other variables were found to correlate significantly with the vortex score. The average nasal index in our sample was indicative of a leptorrhine nose (tall and narrow), which is consistent with the Caucasian race of the majority of our subjects[20]. Besides vortex score, nasal index also significantly correlated ($r=0.62$, $p<0.01$) with measured MCA. However, no correlation between nasal index and nasal surface/volume or nasal resistance was found, replicating findings in previous literature[20;21].

Quantifying Flow Distribution

We quantified and compared the internal flow distributions between individuals by focusing on one coronal slice (#11; see Figure 2b), which was chosen because it cuts through all three (inferior, middle, and superior) turbinates, as well as the olfactory cleft. Since the literature differs on where the major nasal flow peak is located, we first spatially located on each #11 slice the primary airflow peak, as well as the secondary peak, which is defined as a lesser flow peak that is away from the primary peak (see Figure 4a,b). The locations of these peaks for all subjects were then color-coded (red: primary peak; green: secondary peak) onto a generic slice #11 (Figure 4c), which showed considerable spatial variation across individuals: they appeared in the inferior meatus, middle meatus, and lower and upper common meatus (between the turbinates and septum); the only common element was that they never appeared in the superior meatus or the olfactory cleft (Figure 4c).

We further quantified the percentage (fractional) flow rate through different regions of the nasal cavity (olfactory cleft; superior, middle, and inferior regions), as defined in Table 2. Again, there were significant variations in flow rate distributions though these regions across subjects. The most interesting finding is that, on average, there was more airflow through the

middle region than through the inferior region (paired two-tailed t-test, $p<0.05$; Table 2), and the nasal patency rating also significantly correlated with middle meatus flow ($r=-0.65$, $p<0.01$; Table 3). This is surprising given that the inferior turbinate is often thought to be the major contributor to nasal resistance and is the focus of most surgical treatments to relieve nasal obstruction and ensure sufficient airflow through the nasal cavity. However, patency ratings did not correlate with percent flow in the inferior region nor with total nasal resistance. In light of these findings, it may be of equal importance functionally to ensure sufficient flow through the middle meatus region.

No correlation was found between these regional flow percentages and any of the other variables (e.g., total nasal resistance, MCA, nasal index), which indicates that the width of external or internal nasal cavity, or nasal resistance, does not favor flow toward any specific region. This is also surprising, as we often consider the inferior turbinate to be the major regulator to the nasal resistance. During normal nasal cycle, the rhythmic swelling and shrinkage of the erectile tissue throughout the nasal cavity, but most prominently in the inferior turbinate, would create a fluctuation in nasal resistance. In such a case, the percentage of flow surrounding the inferior turbinate would be expected to correlate to the instantaneous nasal resistance: more flow through the inferior region, less congestion and thus less nasal resistance. While we do not have longitudinal data, it is still surprising that across the population at one time point, the inferior turbinate flow percentage is not an indicator of nasal resistance. Percentage flow to the olfactory region is not affected by MCA, nasal resistance, or nasal index with the functional implication that olfactory function is potentially not affected as well.

The significant inverse correlation within these regional flows [e.g., olfactory vs. middle: $r=-0.49$, $p<0.05$; middle vs. inferior: $r=-0.63$, $p<0.01$; Table 3) indicates that different channels are competing for flow: more flow to one region would decrease flow to other regions.

Turbulence Effects

By assuming a turbulence intensity of 2.5%[11] of the mean velocity at the nostril, k-ω turbulence model simulation shows that a moderate level of turbulent airflow continues through the nasal valve region in the restful breathing condition; however, the turbulent energy quickly decays to zero after the nasal valve (Figure 5a). Essentially equivalent velocity profiles were observed visually between the turbulent model and laminar model in the main nasal cavity post-nasal valve. The nasal resistances predicted by laminar or turbulent k-w model closely resemble each other ($r=0.97$, $p<0.01$; see Figure 5b). No significant correlations were found between total turbulent energy (volume weighted) and any other objective and subjective variables, except simulated nasal resistance ($r=-0.49$, $p<0.01$). The correlation with nasal resistance would translate to less nasal resistance associated with higher turbulence energy, which is contrary to a common speculation that high turbulence would result in higher nasal resistance.

Vorticity and Helicity

Vorticity (ξ) is a pseudovector field that measures the local spinning motion of the fluid: $\xi = \nabla \times \vec{V}$, where $\vec{V}$ is the velocity vector; helicity (H) is the inner product of vorticity and velocity $\left(H = \xi \bullet \vec{V}\right)$–vorticity is a vector, whereas helicity is a scalar. Roughly speaking, helicity is a measure of alignment of vorticity with flow direction. In Figure 5c, simulated averaged vorticity magnitude and helicity were plotted against coronal planes. Again, significant variations across the subjects were observed, and vorticity magnitude seemed to peak at the nasal valve region. No correlation was found between the anterior vortex score and total (volume-weighted) vorticity/helicity, or local vorticity value at planes #3 and #4 (corresponding to the general location of the anterior dorsal vortex). No correlations were found between total vorticity and helicity with any other objective or subjective variables. The functional meaning of vorticity and helicity in nasal airflow research thus remains unclear.

Predicting Nasal Patency

We attempt to predict ratings of nasal patency, which has strong clinical relevance, based on all objective variables obtained. As discussed in the Method, since the unilateral patency ratings has already been published[22], here we focused on examining potential relationships between bilateral nasal patency and the additional variables related to internal and external nasal airflow and morphology obtained in this study. Nevertheless, we found that the bilateral ratings significantly correlated ($r=0.91$, $p<0.01$) with the averaged unilateral ratings of the two sides (see Table 2). Initial correlation analysis showed four variables significantly correlated with bilateral nasal patency ratings: middle meatus flow ($r=-0.65$, $p<0.01$), nasal index ($r=0.48$, $p<0.05$), MCA ($r=0.49$, $p<0.05$), and bilateral peak heat loss post-nasal vestibule ($r=-0.51$, $p<0.05$). Bilateral peak nasal heat loss is the larger of the left and right previously reported[17] unilateral peak heat loss. Within these four variables, significant correlation was found between MCA and nasal index, which cannot be entered into a multiple regression analysis at the same time without creating multicollinearity errors, and the inclusion of MCA has a better outcome than does inclusion of the nasal index. The multiple regression analysis then shows that the remaining three variables combined can account for >70% (adjusted $R^2=0.71$, $p<0.01$) of variance of nasal patency ratings among the subjects (Figure 6a, Table 4). This is significant: in comparison, the test-retest reliability of VAS patency rating is around $R^2= 0.56$ or $r=0.75$, $p<0.01$ (Figure 6b).

We further performed a linear discriminant analysis (LDA) [17] to predict subjects' patency rating categories: normal patency versus obstructed patency. As this is a healthy group with a mean bilateral patency rating of 1.8 and a standard deviation of 1.7, we categorized those subjects with ratings less than mean+1 SD as normal (n=17) and those above 1 sd of the mean as moderately obstructed (n=5). LDA was performed using the standard MANOVA approach and showed that two variables combined predicted the patency categories with 86.4% of success rate ($p<0.001$; see Table 5): middle meatus flow percent (most significant) and peak heat loss posterior to the nasal vestibule (see Table 6). The remaining variables were not significant.

DISCUSSION

Results from this study addressed some ongoing controversies in the field regarding normal nasal airflow patterns, especially where the major flow path is located: some past literature indicated major flow along the nasal floor, while a few others suggested middle meatus or common meatus. The results from the present study clarify that such variation coexists normally within a healthy population. The most surprising outcome is the importance of flow in the middle meatus region, which we found on average to be higher than inferior meatus flow, and it correlates significantly with ratings of nasal patency. Taking into account the proximity of middle meatus to the osteomeatal complex, the importance of adequate middle meatus flow warrants further study.

A second ongoing debate regarding normal nasal flow patterns is whether the flow is smooth or has vortices. Keyhani[5] argued that the forming of the anterior dorsal vortex is likely due to individual anatomical variation. As proof, he artificially created an abrupt nasal volume increase after the nasal valve on a model and observed the streamlines changing from smooth into a standing eddy near the olfactory region, similar to Swift and Proctor's report.[2] The present study further confirmed that forming of the anterior dorsal standing vortex is common in a healthy population, and the level of the vortex seems to correlate with nasal index, with narrower and taller external noses more likely to form intense anterior dorsal vortices. However, the functional relevance of such vortex versus smooth airflow pattern is still unclear, as we have yet to find any correlation between the vortex score and total or local turbulence energy/vorticity, or with any other variables examined in this study. The variability of airflow patterns and distributions among individuals indicates that the generalization of results from a single or a few models needs to be cautious. The largest number of subjects involved in any single computational study of normal nasal airflow prior to the present study is four[15].

The occurrence of turbulence in nasal airflow can potentially increase the mixing of air and affect nasal function. In general, a Reynolds number, Re, < 1,500 usually indicates laminar flow, Re > 2,000 indicates turbulence, and 1,500 < Re < 2,000 is transition flow – a mixture of turbulent and laminar flow. Theoretical estimates of the Re of nasal airflow range from 600 (resting breathing) to 2,000 (strong sniffing). However, accurate characterization of nasal airflow turbulence has to come from measurement. Visualizing smoke or dye has been frequently used[14], but this can be misleading because recirculations or eddies also exist in laminar flow and are difficult to distinguish from turbulence eddies. Hot-wire anemometry is probably a more reliable tool to measure turbulence intensity but is difficult to conduct. Based on the available hot-wire anemometry data[11], it is generally agreed that nasal airflow at a restful breathing rate < 200 ml/s is likely predominantly laminar with some transitional flow, while strong sniffing would result in turbulent flow. By assuming a turbulence intensity of 2.5% at the nostril based on the hot-wire anemometry measurement, we used k-ω turbulence model simulation to show that moderate levels of turbulent airflow would continue to the nasal valve region in the restful breathing condition; however, the turbulent energy quickly decays to zero past the nasal valve. Essentially equivalent velocity profiles were observed visually between the turbulence model and laminar model in the main nasal cavity post-nasal valve. Simulated nasal resistances with or without turbulence components

are very similar. Calculated total turbulence energy does not correlate with any other functionally related variables in the present study. Another computational study also suggested that turbulence mixing may have a negligible effect on odorant sorption in the olfactory mucosa[27]. Results suggested that nasal airflow, even during sniffing, is far from fully turbulent, with a ratio of turbulent viscosity to molecular viscosity < 5 (in full turbulence this ratio is >100)[27]. In conclusion, the occurrence of turbulence in nasal airflow is likely confined in the anterior nasal region during restful breathing, and the functional relevance of the turbulence needs to be further examined, possibly case by case for patients and for sniffing conditions.

Similarly, vorticity and helicity, two fundamental concepts in fluid mechanics, have been touted as the potential variables with more physiological and function relevance in nasal airflow research[15;28]. It should be clarified that vorticity does not necessarily mean the existence of vortex or turbulence. The vorticity in perfectly laminar flow (e.g., a straight, long tube) is not zero – actually it is larger near the wall. Many phenomena, such as the blowing out of a candle by a puff of air and the lift force of the airplane wings, are more readily explained in terms of vorticity than by conventional pressure and resistance. Helicity, on the other hand, has a topological interpretation as a measure of linkage and/or knottedness of vortex lines in the flow[29]. It also has many important applications, such as predicting the transfer of vorticity from the environment to an air parcel in convective motion, or predicting the possibility of tornadic development. In the present study, the formation of the strong anterior dorsal vortex does not seem to correlate with total or local vorticity or helicity magnitude. The use of vorticity and helicity in linking nasal airflow and physiological functions awaits more research.

Nasal index, a physical dimension ratio, can be easily obtained, has been found useful in anthropological studies, and thus is an attractive measure if its physiological or clinical values can be identified. One study attempted this but found no correlation to rhinomanometric nasal resistance or to the response to nasal decongestant[20;21]. While replicating this negative finding, we have found three other variables to be significantly correlated with nasal index: vortex score, MCA ($r=0.62$, $p<0.01$), and nasal patency ratings ($r=0.48$, $p<0.05$), which preliminarily indicate its potential value in the rhinology field. However, to be cautious, the external shape of the nose seems not to be the only determining factor for major flow path, as proposed by Grützenmacher et al.[30], since many other flow distribution variables in this study do not correlate with nasal index.

A major critique of the nasal airflow CFD analysis in the past is that few studies[31] directly link the functional relevance of the airflow results. In two previous studies, we tested a hypothesis that the perception of normal, healthy nasal patency, a very important clinical outcome variable, may be mediated by adequate trigeminal sensory input responding to cooling (heat loss) in the nasal mucosa[17;22]. Here we further attempted to predict bilateral perceived nasal patency by combining peak post-vestibule nasal heat loss with MCA and middle meatus region flow percent, which successfully accounted for ~70% of variance of patency using multiple regression and had 86% accuracy in predicting patency categories using LDA. This result does not contradict previous findings, as regional peak mucosal cooling (heat loss) is still one of the most significant variables. Note also that the correlation

between nasal patency and MCA/nasal index – a larger MCA and wider external nose is associated with more congestion perception – is actually the reverse of what we normally expect. However, this correlation may fit our hypothesis nicely: a too-wide nasal passage with the bulk of the airstream having little contact with the mucosal wall may produce a smaller peak in mucosal cooling and the sensation of congestion; a slightly narrower nasal valve would benefit patency by creating strong regional mucosal cooling. The importance of middle meatus flow was unexpected. One possible explanation is that the portion of flow that ends up in the middle meatus may have the best angle to enhance mucosal cooling at the nasal valve region. Because this is a healthy cohort, all analyses can only be viewed as exploratory; more data, especially from patients with nasal obstruction complaints, are necessary to elucidate the contribution of these variables to the perception of nasal patency.

Limitations and Future Work

Only steady inspiratory, restful nasal airflow was considered in the present study; although the restful breathing state is the most common state that we experience in daily life, the effects of strong sniffing and expiratory flow remain to be investigated. Only bilateral variables were analyzed here – bilateral patency is what drives most patients' complaints and thus more clinical relevant, and two of our prior publications have analyzed unilateral patency obtained from the same subject cohort. The protocol of the current study may not capture the effect of the nasal cycle. To do that, a time series of CT scans or, at least, pre- versus post-nasal decongestant CT scans would be needed, which would require new experimental protocols in the future. The bilateral data analysis in our study might mitigate some of the nasal cycle effect, as the two sides often reciprocally congest and decongest, so the unilateral fluctuations would likely cancel each other if summed bilaterally. Indeed, we have seen much better correlation between CFD versus rhinomanometry in bilateral data ($r=0.53$, $p<0.05$) than in unilateral data previously reported ($r=0.41$, $p<0.05$) on the same subject cohort[17]. The population-based analysis might also mitigate some of the nasal cycle effect. The results of the current study would reflect a snapshot among a cohort of subjects who might be in different phases of the nasal cycle, and with a larger sample size than any of the previous literature, the averaged values would have much less fluctuation than individual data in previous literature. Nevertheless, the nasal cycle effect is a limitation of the current study. Racial differences in nasal structure and airflow patterns are also not addressed in this study. We reran our analysis while excluding the two non-Caucasian subjects, and most of the outcomes remained the same; thus, our findings may be preliminarily confined to the Caucasian population. However, starting unprecedented study with a simple racial composition is often necessary to obtain a cleaner result, before expanding to a more diverse racial composition. In summary, the study needs to be replicated with larger sample size; in patients with airway pathologies; with diverse racial composition; with multiple time points to fully capture the nasal cycle effects; and including more complex breathing conditions.

Conclusion

There are significant variations in nasal airflow patterns and properties within the healthy population, and it is difficult to identify a universal template for normal nasal airflow. As clinician and physiologists, we need to focus on nasal functions and to identify nasal airflow

features and variables that may impact those nasal functions. Here we report averages and variations for a range of nasal airflow features within a healthy cohort and attempted to identify a few that may impact nasal patency perception. Collections of these normative data can potentially be translated to clinical populations to formulate hypothesis and to understand the impact of changes due to pathological consequences on the nasal airflow and the targeted nasal functions.

Acknowledgments

Thanks to Dr. Pamela Dalton (Monell) for providing critiques to the manuscript, Dr. Edmund Pribitkin and Chris Klock (Thomas Jefferson Hospital) for facilitating institutional review board approval and CT scans, and Kara Blacker and Yuehao Luo (Monell) for help with experiments and data collection.

Funding support: NIH 5R03DC008187

Reference List

1. Zhao K, Dalton P. The way the wind blows: implications of modeling nasal airflow. Curr Allergy Asthma Rep. 2007; 7:117–125. [PubMed: 17437682]
2. swift, DL.; Proctor, DF. Access of air to the respiratory tract.. In: Brain, JD.; Proctor, DF.; Reid, LM., editors. Respiratory defense mechanism. Marcel Dekker Inc.; New York: 1977. p. 63-91.
3. Simmen D, Scherrer JL, Moe K, Heinz B. A dynamic and direct visualization model for the study of nasal airflow. Arch Otolaryngol Head Neck Surg. 1999; 125:1015–1021. [PubMed: 10488989]
4. Elad D, Liebenthal R, Wenig BL, Einav S. Analysis of air flow patterns in the human nose. Med Biol Eng Comput. 1993; 31:585–592. [PubMed: 8145584]
5. Keyhani K, Scherer PW, Mozell MM. Numerical simulation of airflow in the human nasal cavity. J Biomech Eng. 1995; 117:429–441. [PubMed: 8748525]
6. Kelly JT, Prasad AK, Wexler AS. Detailed flow patterns in the nasal cavity. J Appl Physiol. 2000; 89:323–337. [PubMed: 10904068]
7. Chung SK, Son YR, Shin SJ, Kim SK. Nasal airflow during respiratory cycle. Am J Rhinol. 2006; 20:379–384. [PubMed: 16955764]
8. Zhao K, Scherer PW, Hajiloo SA, Dalton P. Effect of anatomy on human nasal air flow and odorant transport patterns: implications for olfaction. Chem Senses. 2004; 29:365–379. [PubMed: 15201204]
9. Subramaniam RP, Richardson RB, Morgan KT, Kimbell JS. Computational fluid dynamics simulations of inspiratory airflow in the human nose and nasopharynx. Inhal Toxicol. 1999; 10:91–120.
10. Proctor DF. Nasal mucociliary function in humans (5 ed.). 1977:427–452.
11. Hahn I, Scherer PW, Mozell MM. Velocity profiles measured for airflow through a large-scale model of the human nasal cavity. J Appl Physiol. 1993; 75:2273–2287. [PubMed: 8307887]
12. Hornung DE, Leopold DA, Youngentob SL, et al. Airflow patterns in a human nasal model. Arch Otolaryngol Head Neck Surg. 1987; 113:169–172. [PubMed: 3801173]
13. Schreck S, Sullivan KJ, Ho CM, Chang HK. Correlations between flow resistance and geometry in a model of the human nose. J Appl Physiol. 1993; 75:1767–1775. [PubMed: 8282630]
14. Churchill SE, Shackelford LL, Georgi JN, Black MT. Morphological variation and airflow dynamics in the human nose. Am J Hum Biol. 2004; 16:625–638. [PubMed: 15495233]
15. Segal RA, Kepler GM, Kimbell JS. Effects of differences in nasal anatomy on airflow distribution: a comparison of four individuals at rest. Ann Biomed Eng. 2008; 36:1870–1882. [PubMed: 18777212]
16. Zhu JH, Lee HP, Lim KM, Lee SJ, Wang dY. Evaluation and comparison of nasal airway flow patterns among three subjects from Caucasian, Chinese and Indian ethnic groups using computational fluid dynamics simulation. Respir Physiol Neurobiol. 2011; 175:62–69. [PubMed: 20854936]

17. Zhao K, Jiang J, Blacker K, et al. Regional peak mucosal cooling predicts the perception of nasal patency. Laryngoscope. 2013
18. Clement PA. Committee report on standardization of rhinomanometry. Rhinology. 1984; 22:151–155. [PubMed: 6505516]
19. Thomson A, Buxton LHD. Man's nasal index in relation to certain climatic conditions. The J of the Royal Anthropol Institute of Great Britain andIreland. 1923; 53:92–122.
20. Leong SC, Eccles R. A systematic review of the nasal index and the significance of the shape and size of the nose in rhinology. Clin Otolaryngol. 2009; 34:191–198. [PubMed: 19531167]
21. Doddi NM, Eccles R. The relationship between nasal index and nasal airway resistance, and response to a topical decongestant. Rhinology. 2011; 49:583–586. [PubMed: 22125790]
22. zhao, k; blacker, k; luo, y; bryant, b; Jiang, J. Perceiving nasal patency through mucosal cooling rather than air temperature or nasal resistance. Plos One. 2011; 6:e24618. [PubMed: 22022361]
23. Wilcox, DC. Turbulence modeling for CFD. 3rd ed.. DCW Industries; 2006.
24. Warren DW, Walker JC, Drake AF, Lutz RW. Assessing the effects of odorants on nasal airway size and breathing. Physiol Behav. 1992; 51:425–430. [PubMed: 1557452]
25. Moore EJ, Kern EB. Atrophic rhinitis: a review of 242 cases. Am J Rhinol. 2001; 15:355–361. [PubMed: 11777241]
26. Eccles R. Nasal airflow in health and disease. Acta Otolaryngol. 2000; 120:580–595. [PubMed: 11039867]
27. Zhao K, Dalton P, Yang GC, Scherer PW. Numerical Modeling of Turbulent and Laminar Airflow and Odorant Transport during Sniffing in the Human and Rat Nose. Chem Senses. 2006; 31:107–118. [PubMed: 16354744]
28. Ishikawa S, Nakayama T, Watanabe M, Matsuzawa T. Visualization of flow resistance in physiological nasal respiration: analysis of velocity and vorticities using numerical simulation. Arch Otolaryngol Head Neck Surg. 2006; 132:1203–1209. [PubMed: 17116815]
29. Moffatt HK. The degree of knottedness of tangled vortex lines. J Fluid Mech. 1969; 35:117–129.
30. Grutzenmacher S, Robinson DM, Lang C, Lebe E, Knape U, Mlynski G. Investigations of the influence of external nose deformities on nasal airflow. ORL J Otorhinolaryngol Relat Spec. 2005; 67:154–159. [PubMed: 15925912]
31. Zhao K, Pribitkin EA, Cowart BJ, Rosen D, Scherer PW, Dalton P. Numerical modeling of nasal obstruction and endoscopic surgical intervention: outcome to airflow and olfaction. American Journal of Rhinology. 2006; 20:308–316. [PubMed: 16871935]

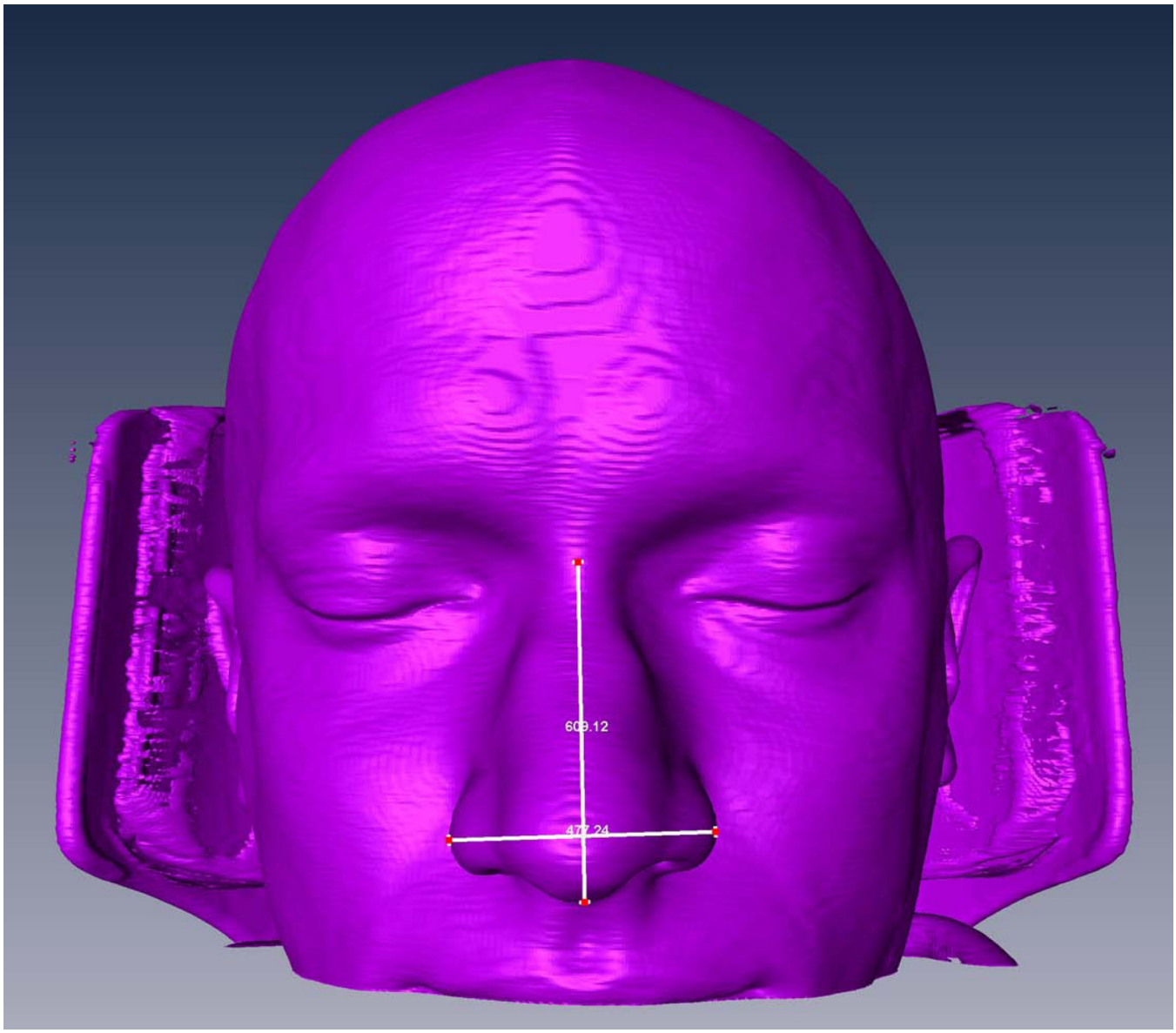

Figure 1.
Facial reconstruction based on CT scan, and measurement of nasal index.

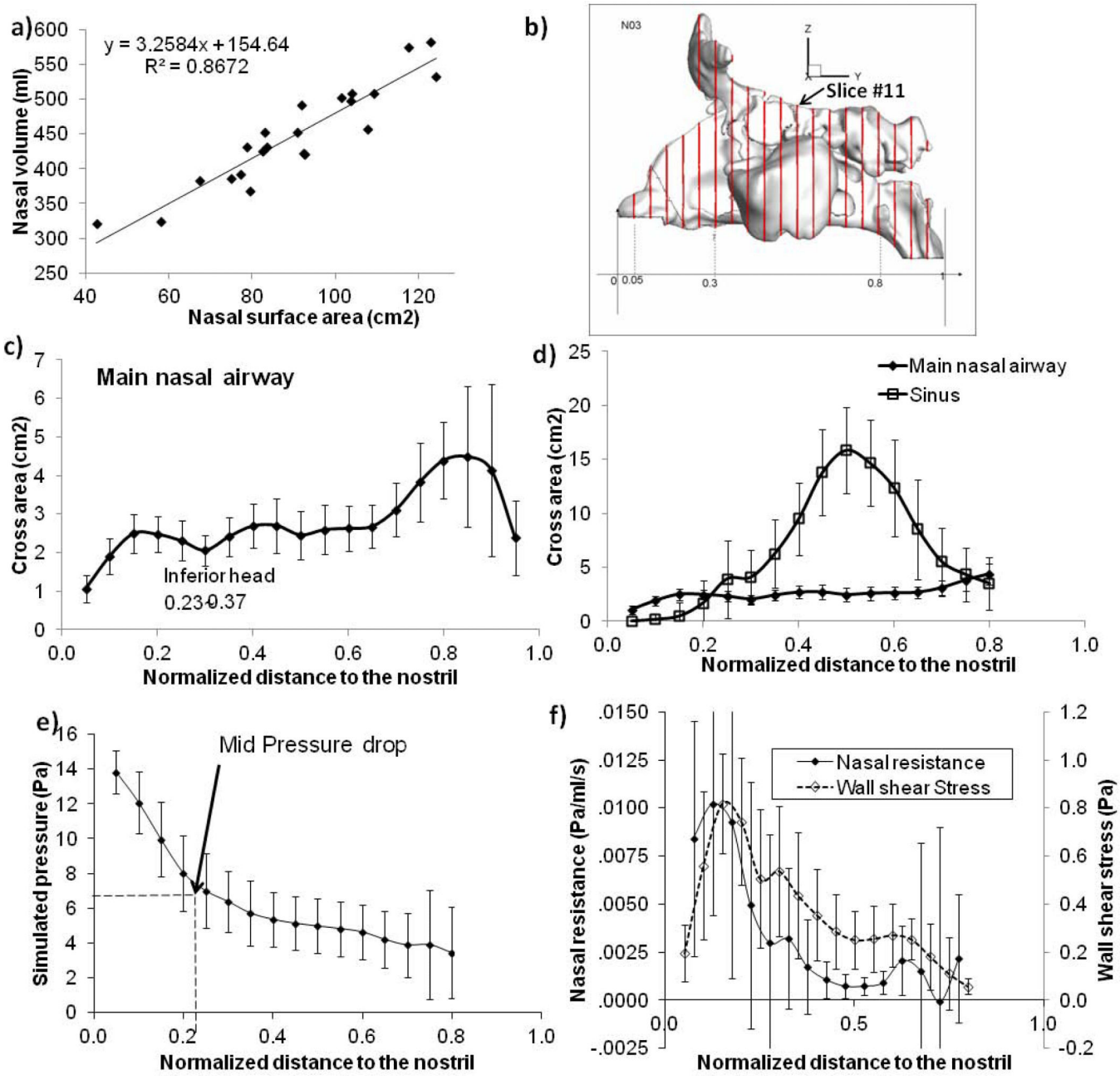

Figure 2.

(a) Nasal airway volume and surface area (excluding sinus and nasal pharynx) significantly correlate with each other. (b) To account for difference in overall lengths of different individual, each nasal cavity is sectioned into 19 uniformly spaced coronal planes. The average length of nasal cavity was 11.2 cm, and each plane was spaced on average 0.56 cm. The last three coronal sections that cut through the nasopharynx region were excluded from the analysis. (c and c) Average and standard deviation of cross-sectional area of main nasal airway (a) and sinus (b) of the CFD models as a function of normalized distance to the nostril. (e and f) Average (area-weighted) and standard deviation of pressure drop (e) and regional nasal resistance (f) as a function of distance to the nostril.

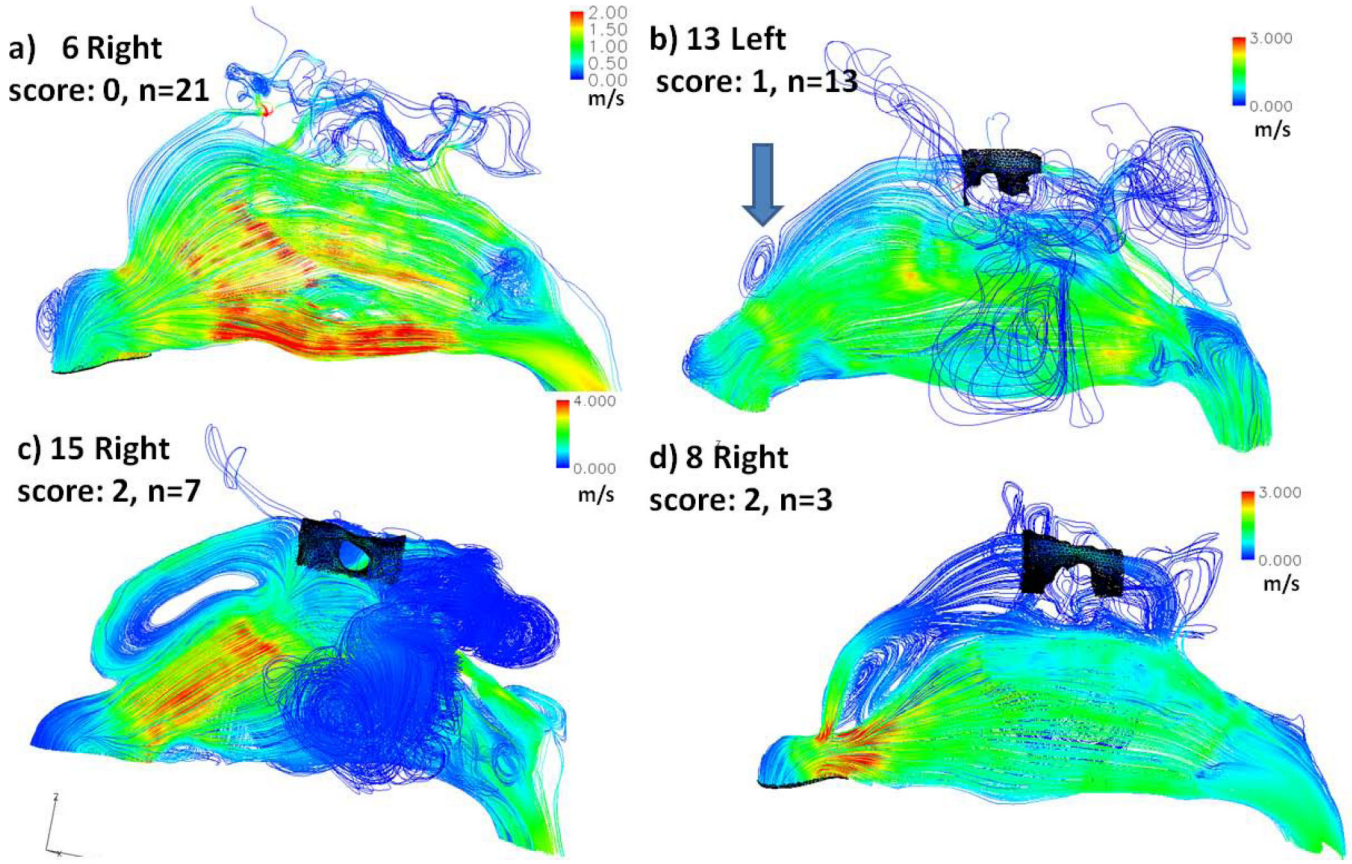

Figure 3.

Examples of streamline patterns and formation of the anterior dorsal vortex: (a) no vortex, (b) a small vortex, (c) a significant vortex, and (d) a significant vortex but in clockwise rotation. The intensity of the vortex is further scored 0 for no vortex (a), 1 for small vortex (b), 2 for large vortex (c and d); n-values indicate the number of sides that were categorized into each pattern. Black shade indicates the olfactory region.

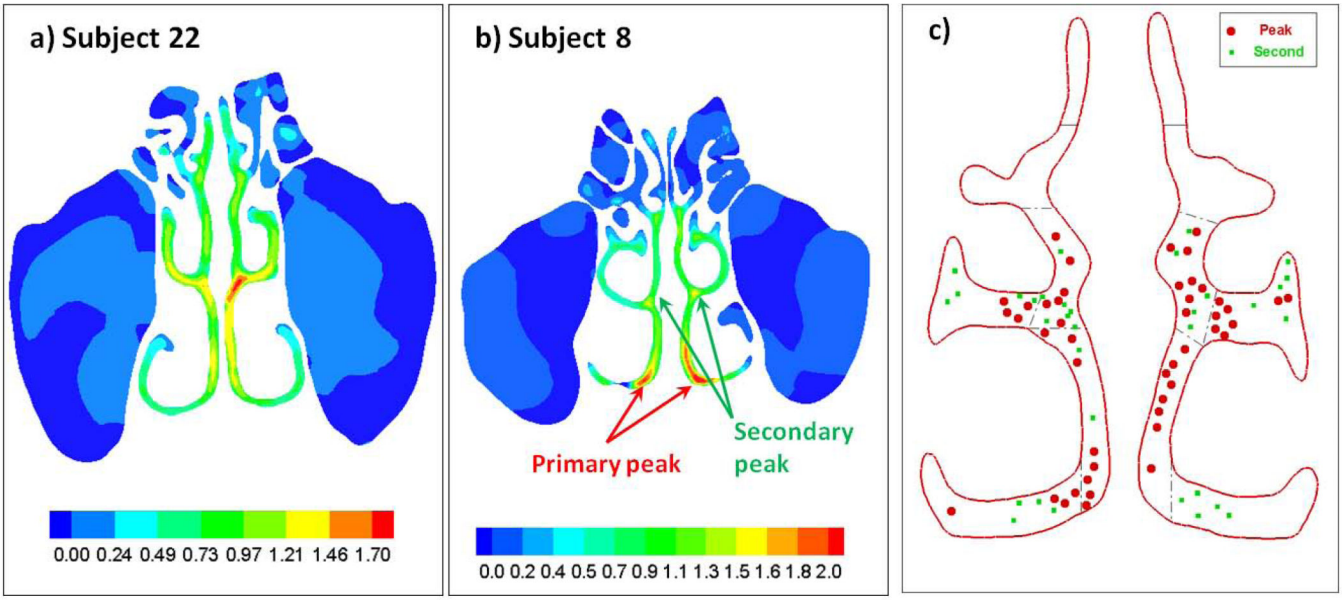

Figure 4.

(a and b) Examples of variations in internal flow distributions for two subjects – velocity contour plots on coronal slice (#11) and the location of the primary flow peak and secondary flow peak (defined as a lesser flow peak away from the primary peak). This slice was chosen because it cuts through all three (inferior, middle, and superior) turbinates, as well as the olfactory cleft. (c) The locations of these peaks of all subjects were then color-coded (red: primary peak; green: secondary peak) onto a generic cross-sectional plane #11. The primary and secondary peaks showed considerable spatial variation across individuals, appearing in the inferior meatus, middle meatus, and lower and upper common meatus, with the only common feature that they never appeared in the superior meatus or the olfactory cleft.

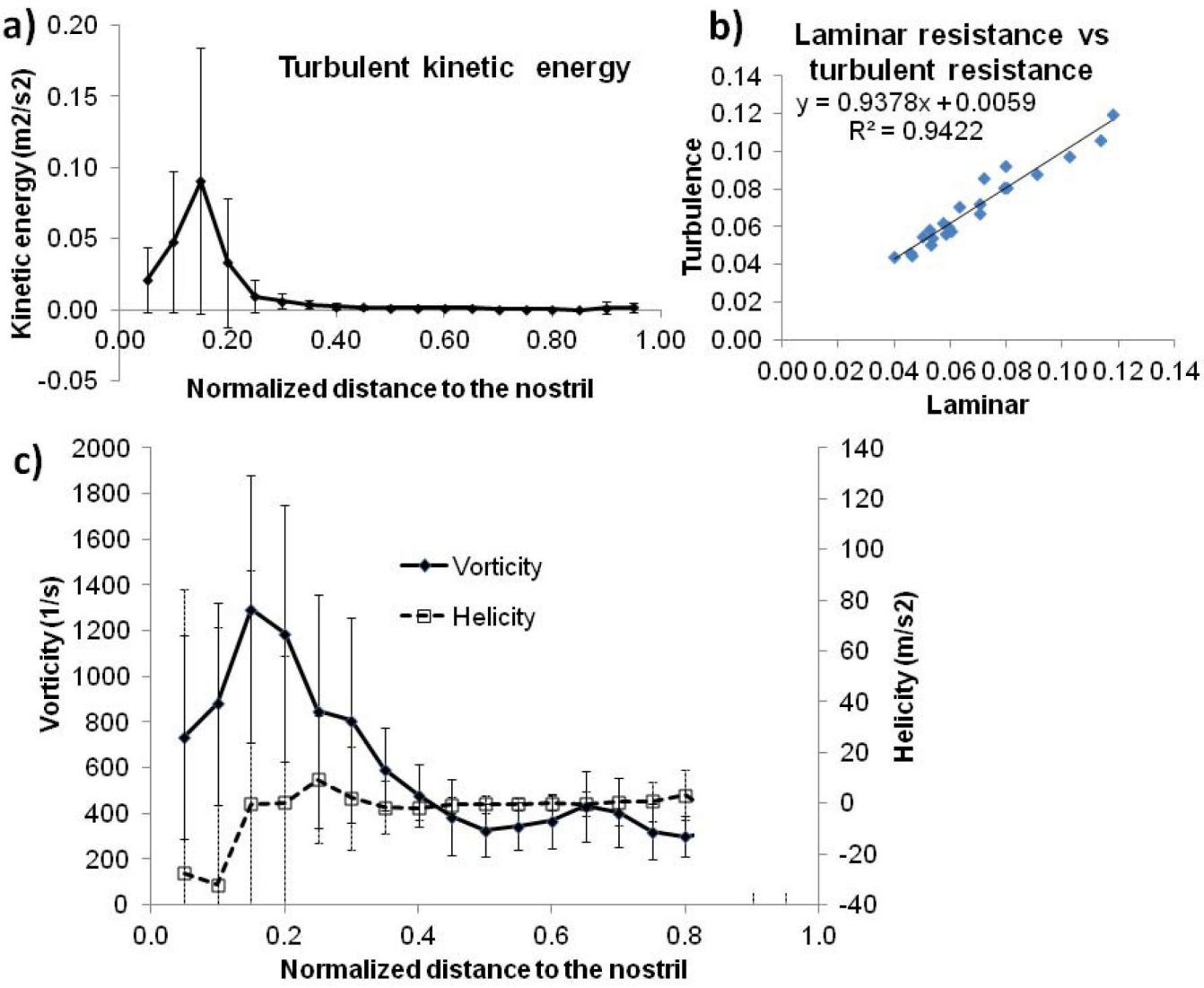

Figure 5.

(a and c) Average (area-weighted) and standard deviation of turbulence kinetic turbulence energy (a) and vorticity and helicity (c) as a function of distance to the nostril. (b) Simulated nasal resistances by laminar and turbulence k-ω models strongly correlated ($r=0.92$, $p<0.01$).

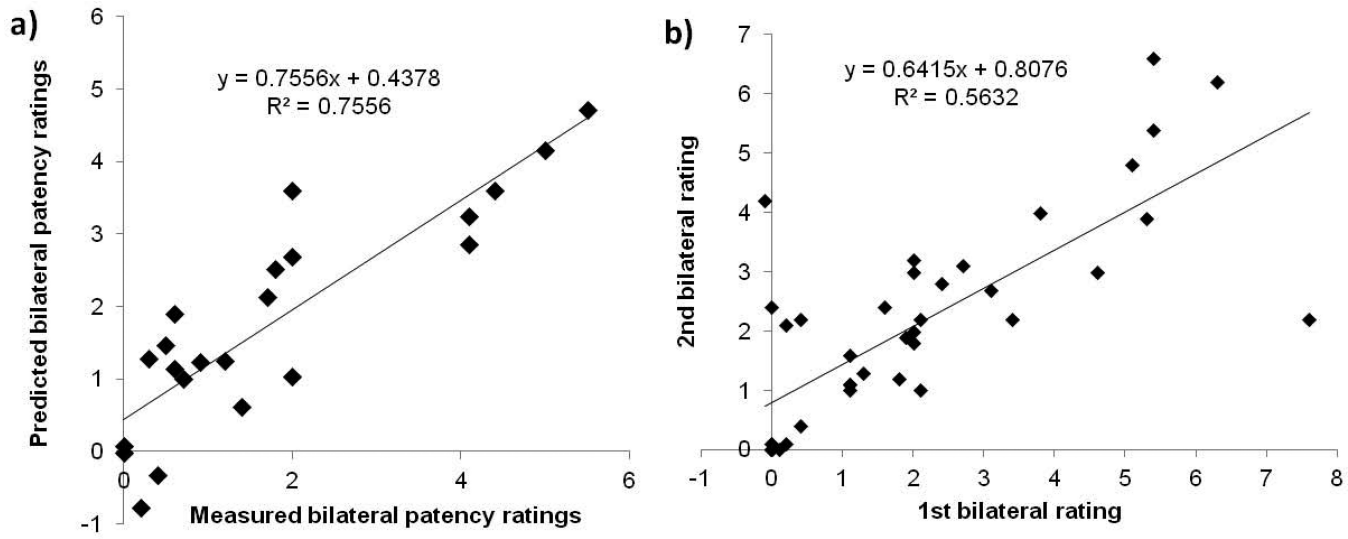

Figure 6.

(a) Predicted bilateral patency ratings based on multiple regression model (adjusted R^2=0.71, p<0.01) (see Table 4) versus measured VAS patency rating. (b) Test-retest reliability of VAS bilateral patency rating (R^2=0.56 or r=0.75, p<0.01).

Table 1

Subject nasal biometrics

Subject	Gender	Race	Volume (ml)	Surface area (cm^2)	Nasal index
N02	F	Caucasian	78.65	431.04	0.67
N03	F	Caucasian	77.14	392.34	0.70
N04	M	Caucasian	124.14	533.10	0.77
N05	F	Caucasian	75.08	386.88	0.72
N06	M	Caucasian	122.84	582.72	0.72
N07	M	Afr. Amer.	58.05	324.98	0.83
N08	F	Caucasian	82.45	425.19	0.66
N09	M	Caucasian	92.71	421.43	0.79
N10	F	Caucasian	117.53	574.65	0.59
N11	F	Asian	92.35	422.84	0.60
N12	M	Caucasian	91.93	492.16	0.83
N13	M	Caucasian	104.01	508.77	0.74
N14	M	Caucasian	109.20	508.49	0.87
N15	F	Caucasian	79.58	368.70	0.61
N16	F	Caucasian	67.37	382.92	0.72
N18	F	Caucasian	90.92	452.00	0.71
N19	F	Caucasian	42.64	321.70	0.63
N20	M	Caucasian	82.96	451.98	0.68
N21	M	Caucasian	107.71	457.80	0.78
N22	F	Caucasian	103.65	498.17	0.60
N23	F	Caucasian	83.57	431.67	0.73
N24	M	Caucasian	101.32	502.94	0.67
Mean			90.26	448.75	0.71
SD			20.42	71.46	0.08
N05	F	Caucasian	75.08	386.88	0.72
N06	M	Caucasian	122.84	582.72	0.72
N07	M	Afr. Amer.	58.05	324.98	0.83
N08	F	Caucasian	82.45	425.19	0.66
N09	M	Caucasian	92.71	421.43	0.79
N10	F	Caucasian	117.53	574.65	0.59
N11	F	Asian	92.35	422.84	0.60
N12	M	Caucasian	91.93	492.16	0.83
N13	M	Caucasian	104.01	508.77	0.74
N14	M	Caucasian	109.20	508.49	0.87
N15	F	Caucasian	79.58	368.70	0.61
N16	F	Caucasian	67.37	382.92	0.72
N18	F	Caucasian	90.92	452.00	0.71
N19	F	Caucasian	42.64	321.70	0.63
N20	M	Caucasian	82.96	451.98	0.68

Subject	Gender	Race	Volume (ml)	Surface area (cm^2)	Nasal index
N21	M	Caucasian	107.71	457.80	0.78
N22	F	Caucasian	103.65	498.17	0.60
N23	F	Caucasian	83.57	431.67	0.73
N24	M	Caucasian	101.32	502.94	0.67
Mean			90.26	448.75	0.71
SD			20.42	71.46	0.08

Table 2

Percentage (fractional) of flow through different regions (olfactory cleft, superior, middle, and inferior regions) of the nasal cavity. On average, more air flowed through the middle region than through the inferior region (paired two-tailed t-test, $p<0.05$), and middle meatus flow % was significantly correlated with the nasal patency rating ($r=-0.65$, $p<0.01$).

	Subject	Olfactory cleft	Superior	Middle	Inferior	Resistance (Pa*S/ml, CFD, simulation)	Resistance (Pa*S/ml, measured)	Patency bilateral	Patency (unilateral averaged)
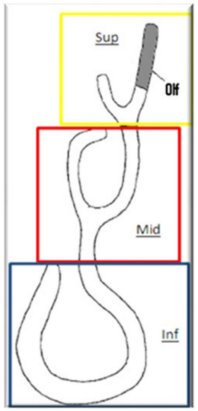	2	4.7%	14.1%	49.4%	36.5%	0.072	0.074	0.3	1.15
	3	2.1%	5.4%	58.9%	35.7%	0.053	0.062	0	1
	4	0.9%	3.6%	46.2%	50.2%	0.046	0.036	1.8	2.4
	5	14.4%	32.2%	29.9%	38.0%	0.05	0.060	4.1	3.2
	6	4.4%	20.7%	41.2%	38.0%	0.057	0.043	4.4	4.75
	7	16.1%	38.2%	26.1%	35.7%	0.102	0.047	5.5	4.7
	8	1.2%	2.8%	44.4%	52.8%	0.08	0.089	0.5	0.6
	9	1.1%	2.6%	70.9%	26.5%	0.118	0.074	1.4	1.25
	10	0.4%	1.0%	38.0%	61.0%	0.091		0.4	0.25
	11	5.6%	15.2%	60.0%	24.7%	0.113	0.170	0.2	1.25
	12	2.9%	15.9%	46.8%	37.3%	0.08	0.073	1.7	2.6
	13	2.2%	7.6%	61.7%	30.7%	0.058	0.044	2	3.5
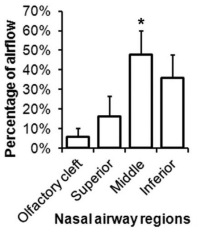	14	7.4%	25.0%	34.5%	40.6%	0.071	0.060	2	1.85
	15	4.7%	18.3%	64.8%	17.0%	0.054	0.056	0	—0.05
	16	6.1%	18.2%	52.9%	29.0%	0.063	0.078	0.9	0.6
	18	6.0%	13.7%	55.4%	30.9%	0.06	0.074	0.7	1.2
	19	5.3%	14.1%	55.4%	30.6%	0.079	0.088	1.2	1.7
	20	5.5%	11.4%	26.1%	62.5%	0.071	0.057	5	5.7
	21	7.6%	19.4%	50.4%	30.1%	0.046	0.058	4.1	3.95
	22	11.0%	28.9%	43.6%	27.6%	0.059	0.041	0.6	0.85
	23	11.3%	30.3%	50.3%	19.4%	0.053	0.028	0.6	2.35
	24	7.9%	19.7%	46.8%	33.5%	0.04	0.047	2	1.45
	Average	5.8%	16.3%	47.9%	35.8%	0.069	0.065	1.80	2.10

	Subject	Olfactory cleft	Superior	Middle	Inferior	Resistance (Pa*S/ml, CFD, simulation)	Resistance (Pa*S/ml, measured)	Patency bilateral	Patency (unilateral averaged)
	SD	4.3%	10.3%	12.1%	11.8%	0.022	0.029	1.71	1.59

*On average, more air flowed through the middle region than through the inferior region (paired 2-tailed *t* test, $p < 0.05$), and middle meatus flow percentage significantly correlated with the bilateral nasal patency rating (r =—0.65, $p < 0.01$). Bilateral patency significantly correlated with the averaged unilateral patency from the two sides ($r = 0.91$, $p < 0.01$). Rhinomanometry measured nasal resistance correlated significantly with CFD simulated ones ($r = 0.53$, $p < 0.01$), however, none of the resistances correlated with patency ratings. SD = standard deviation.

Table 3

Pearson and Spearman rank [in ()] correlation matrix between all variables. Values shown are those for correlation coefficients r>0.3 (accounting for at least 9% of total variance) and p<0.05; * indicates p<0.01; (ns) indicates not significant.

	Middle meatus flow %	**Inferior meatus flow %**	**Nasal index**	**Resistance (CFD, laminar)**	**Resistance (measured)**	**MCA (L+R)**	**Patency rating**	**Turbulence energy**
Olfactory flow percent	−**0.49*** (ns)						0.46 (ns)	
Middle meatus flow percent		− **0.63* (− 0.74)**					− **0.65* (− 0.53)**	
Inferior meatus flow percent								
Nasal index						**0.62*** (0.68)	0.48 (0.63)	
Resistance (CFD)					0.53 (0.63)			−0.49 (−0.53)
Resistance (measured)								
MCA (L+R)							0.49 (0.65)	
Patency rating								

Variables that correlated with only one other variable are not included in the table: Nasal volume vs. surface area, r=0.93, p<0.01. Peak heat loss post nasal vestibule vs. patency ratings, r =-0.51, p< 0.05. Anterior vortex score vs. nasal index, r=-0.46, p<0.05.

Table 4

Multiple regression: Predicted bilateral nasal patency = 2.04 × MCA − 0.00137 × peak heat loss (post-vestibule) − 8.17 × middle flow percent + 5.8; R^2=0.76, adjusted R^2=0.71. F(3,18)=18.5, p<0.0001*. (see also Figure 6a).

	b	SE *b*	Partial correlation	p-Value
Intercept				0.001
Middle meatus flow (CFD)	−0.62	0.12	−0.77	0.000
MCA	0.41	0.12	0.63	0.003
Peak nasal heat loss (post-vestibule, CFD)	−0.29	0.12	−0.49	0.028

R^2 measures the reduction in the total variation of the dependent variable due to the (multiple) independent variables, adjusted R^2 takes into consideration the number of degrees of freedom and is adjusted by dividing the error sum of squares and total sums of square by their respective degrees of freedom (R^2 (adjusted) = 1 − [(residual SS/df)/(total SS/df)]; and the F-value and resulting p-value are used as an overall F-test of the relationship between the dependent variable and the set of independent variables (here F = regression mean square/residual mean square). *b* is* the normalized regression coefficient for the variable in the regression equation. The *SE b* is* the estimated standard error of the regression coefficient. Partial correlation is a correlation between two variables after controlling for other variables.

Table 5

Linear discriminant analysis (LDA) classification matrix: predicted versus actual patency category (n=22).

Patency Rating	Predicted Patency		Percent correct
	Normal	Obstructed	
Normal	16	1	94.1%
Obstructed	2	3	60%
Total			86.4%

Table 6

Wilks' lambda and univariate (F) tests of equality of group means, probability value, and lambda for the two significant variables in LDA classification analysis.Significant variable

Significant variables	Wilks' lambda	F(1, 19)	p-Value	Partial lambda
Middle meatus flow percent	0.82	11.3	0.003*	0.63
Peak heat loss (post-vestibule, CFD)	0.63	4.48	0.048*	0.81

Wilks' lambda is a multivariate equivalent of the ANOVA (F) test of mean differences in LDA, such that the smaller the lambda for an independent variable, the more that variable contributes to the discriminant function. Lambda varies from 0 to 1, with 0 explaining 100% of the variability and 1 explaining 0% of the variability. Partial lambda is a measure of how much variability is accounted for by each individual variable by itself while ignoring the contribution of the other variables. Here, middle meatus flow percent can explain the most variability by itself, followed by peak heat loss.